Optimization of ultrasonic-assisted green synthesis of Au-ZnO bimetallic nanoparticles using pineapple (Ananas comosus) peels extract

April Mergelle R. Lapuz*, Julius D.G. Contreras, Queenzy T. Trinidad, Jenela Mae F. Bañes, Farha E. Nour, and Jerome D. Fundano

College of Pharmacy, Adamson University, Ermita, Manila, Metro Manila 1000, Philippines

ABSTRACT

imetallic nanoparticles are composed of two metals with specific activities that produce a greater effect when combined. Gold and zinc oxide nanoparticles provide various pharmacological applications such as antibacterial, anticancer, antimicrobial, and antioxidant. In the biosynthesis of bimetallic nanoparticles, appropriate temperature and power are the factors evaluated to produce optimized bimetallic nanoparticles (BNPs) using a certain synthesis method. This study aimed to determine the optimum temperature (Celsius) and sonication power (watts) for the green synthesis of Au-ZnO bimetallic nanoparticles by the phenolic compounds contained in *Ananas comosus* peels extract as reducing and capping agents using an ultrasonic-assisted method.

The *A. comosus* peels were collected, dried, and extracted using 95% ethanol and water (50:50). The extract was then tested using ferric chloride and potassium dichromate to confirm the presence of phenolic compounds. The Au-ZnO BNPs were green-synthesized under varying temperatures (60 - 80°C) and sonication power (60 - 180 watts). The Au-ZnO BNPs were characterized using UV-Vis spectroscopy, SEM-EDX, and FTIR. The BNPs were also subjected to *in vitro* assays for DPPH scavenging activity and UV protection property.

Results indicated that the absorbance peaks at 315 nm and 545 nm for ZnO NPS and Au NPS while the Au-ZnO NPS obtained from different temperatures and sonication power showed characteristic peaks between 320 to 345 nm and between 530 to 540 nm, respectively. The inhibitory concentration (IC₅₀) for the DPPH scavenging activity for Au NPS, ZnO NPS, and the Au-ZnO BNPs were calculated to be 346.38, 67.68, and 11.26 – 808.68 µg/mL, respectively. The Au-ZnO BNPs C1, C4, C7, and C9 showed good UV protection properties with UPF values 18.96, 18.08, 14.79, and 17.02, respectively. Results of the optimization indicated that the Au-ZnO BNPs synthesized under low temperature (60°C) and low sonication power (60 watts) exhibited the highest DPPH scavenging activity and UV protection property.

INTRODUCTION

Nanotechnology is a promising technological advancement of the 21st century, with vast applications in various fields, including medicine (Abdussalam-Mohammed 2019). It involves the manipulation and manufacturing of materials at a nanometer scale, typically between 1nm to 100nm, using nanoscience theory (Bayda et al. 2019; Micheletti and Venturini 2015). In pharmacy, nanotechnology plays a vital role in drug delivery, diagnostic devices, and biosensors, offering solutions to common challenges such as drug solubility, efficacy, and elimination (Bisso and Leroux 2020).

Compared to macroparticles, nanoparticles (NPs) provide distinct advantages in drug delivery, including reduced side

KEYWORDS

Optimization, bimetallic nanoparticles, pineapple peels, green synthesis

*Corresponding author

Email Address: april.mergelle.lapuz@adamson.edu.ph

Date received: 31 October 2024 Date revised: 16 May 2025

Date accepted: 23 September 2025

DOI: https://doi.org/10.54645/202518SupHIF-53

effects, enhanced bioavailability, and improved tissue penetration (Ak et al. 2014; Al-Jbour 2022; Wilhelm et al. 2016). Key factors such as particle size and shape influence pharmacokinetics, biodistribution, and tissue penetration (Ernsting et al. 2013; Xu et al. 2023). Bimetallic nanoparticles (BNPs), composed of two metals, have gained attention due to their superior properties, including improved catalytic activity and more active sites (Berta et al. 2021; Cao et al. 2015).

Among nanoparticles, gold (Au) and zinc oxide (ZnO) nanoparticles have been widely used in biomedical and pharmacological applications due to their low toxicity and protective properties (Milanezi et al. 2019). Recent studies related to the toxicity of Au and ZnO nanoparticles provide little information regarding their health effects on humans. Some in vivo toxicity studies of AuNPs include their systemic accumulation in different organs, while ZnO NPs are found to be safe at certain levels and may only cause toxicity at higher concentrations (Nagar et al. 2022; Sani et al. 2021). Moreover, physicochemical properties of nanoparticles such as size and shape affect its uptake and removal behavior (Ding et al. 2018), which are significant in the determination of their activity and toxicity. The toxicity problem associated with nanoparticles demands a comprehensive approach that involves progressive methodologies and the incorporation of green synthesis principles. (Niżnik et al. 2024). Notably, gold nanoparticles have demonstrated antioxidant and antibacterial activity, while zinc oxide nanoparticles show anti-inflammatory, antioxidant, and UV protection properties (Pal et al. 2013; Mirzaei and Darroudi 2017). These properties make gold-zinc oxide bimetallic nanoparticles (Au-ZnO BNPs) a valuable candidate for synthesis in pharmaceutical applications (Padilla-Cruz et al. 2021).

Traditional nanoparticle synthesis methods, such as chemical and physical synthesis, have drawbacks, including the use of toxic chemicals and high energy consumption (Nasrollahzadeh et al. 2019; Iravani et al. 2014). To address these issues, green synthesis has emerged as an environmentally friendly alternative, utilizing natural sources like microorganisms, and biowaste materials to synthesize nanoparticles (Parveen et al. 2016; Afreen et al. 2020). Biowaste materials, such as fruit peels, provide a sustainable source for nanoparticle synthesis due to their high content of beneficial bioactive compounds (Rodriguez-Félix et al. 2022). Pineapple peels, in particular, contain significant amounts of phenolic compounds that act as reducing and capping agents during nanoparticle synthesis (Romelle et al. 2016; Pechyen, et al., 2021). Phenolic compounds donate electrons to reduce metal ions to nanoparticles and prevent aggregation, which is essential for controlling nanoparticle size and stability (Iravani 2011). While other plant peels, such as banana, mango, and pomegranate, also contain phenolics, pineapple peels provide a significant amount and are more readily accessible for use in green nanoparticle synthesis (Vu et al. 2018; Sulaiman et al. 2018). Various Philippine fruit peels, such as sugar apple, banana, cotton fruit, mango, and pineapple, were tested for their phenolic compounds, and all yielded positive results, indicating a significant presence of these bioactive compounds (Pates et al. 2024).

Different environmental factors and handling practices can affect the phenolic content of pineapple peel waste. However, the extraction of their phenolic content is highly enhanced by certain drying and extraction processes (Dewi et al. 2023). This study focused on the qualitative determination of phenolic compounds from pineapple peels for the synthesis of Au-ZnO BNPs.

The use of ultrasonication in green synthesis further enhances the extraction and synthesis of nanoparticles. Ultrasonication aids in the extraction of phenolic compounds by breaking down cell barriers and reducing the required extraction time (Wahab and Yahya 2019; Wang et al. 2015; Freitas de Oliveira et al. 2016). This technique also prevents nanoparticle agglomeration and enhances dispersion, resulting in high-quality nanoparticles with better stability and activity (Khairunnisa et al. 2021).

Several factors, including temperature and ultrasonic power, significantly affect the physicochemical properties of biosynthesized BNPs. Higher temperatures and ultrasonic power can increase nanoparticle yield and efficiency, but excessive heat may lead to the decomposition of phytochemicals and agglomeration of nanoparticles (Makarov et al. 2014; Cruz et al. 2010; Satpathy et al. 2020; Karadirek and Okkay 2019; Gao et al. 2022). Temperature and ultrasonic power were selected as the primary factors for optimization, as both parameters critically influence the size, morphology, and purity of the synthesized nanoparticles. Previous studies have shown that increasing reaction temperature and sonication power lead to smaller particle sizes, more uniform morphology, and reduced aggregation and impurities (Tajally et al. 2008; Tohidi et al. 2022). This relationship exists because these factors directly affect cavitation intensity and reaction kinetics, thereby making temperature and ultrasonic power key variables in the ultrasonicassisted green synthesis of nanoparticles.

While numerous studies have explored the green synthesis of monometallic nanoparticles using various plant materials, there is a notable scarcity of research focusing on the ultrasonicassisted green synthesis of Au-ZnO bimetallic nanoparticles (BNPs) utilizing pineapple peel extract. Existing literature predominantly addresses monometallic systems or employs different plant extracts, often without comprehensive optimization of critical synthesis parameters such as temperature and sonication power to enhance biological properties. This study addressed this gap by employing a sustainable biowaste as a reducing and stabilizing agent in the ultrasonic-assisted synthesis of Au-ZnO BNPs. By systematically optimizing synthesis conditions, the research enhances the antioxidant and UV-protective properties of the nanoparticles, offering a sustainable approach with potential pharmaceutical applications. This methodological advancement not only promotes eco-friendly practices but also contributes novel insights into the synthesis of high-performance BNPs, distinguishing this study from prior works in the field.

The results of this study provide insights into the potential pharmaceutical applications of green-synthesized bimetallic nanoparticles, particularly in developing dosage forms with BNPs as active ingredients. Furthermore, this research highlights the sustainability of using biowaste for green synthesis.

MATERIALS AND METHODS

Materials

The zinc acetate (Zn(CH₃COO)₂), titanium oxide (TiO₂), and chloroauric acid were purchased from Jinan Future Chemical Co., Ltd. The ascorbic acid and DPPH reagent were from DKL Laboratories. The 95% ethanol was obtained from Puljed Trading Medical and Laboratory Supply, while the deionized water, ferric chloride, and potassium dichromate were from Adamson University College of Pharmacy.

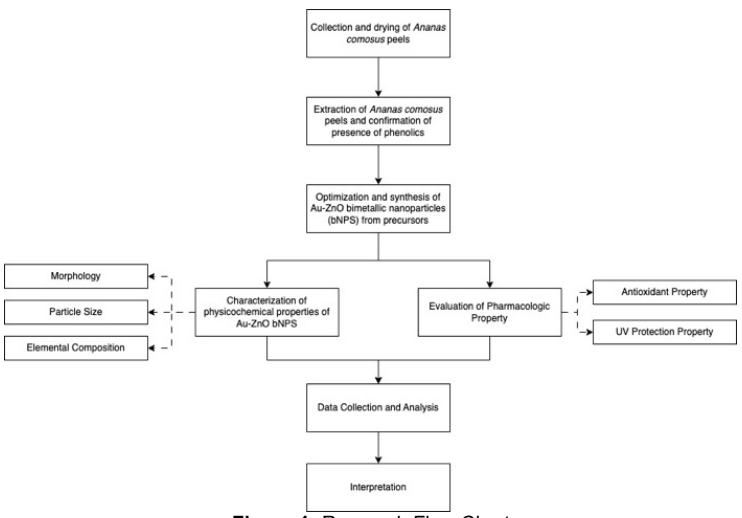


Figure 1: Research Flow Chart

Preparation of samples

The fresh pineapple peels collected as waste from the local market (Paco, Manila) were washed to remove the dirt, then the peels were dried in the oven at 60°C, ground, and sifted through a 40-mesh sieve in preparation for the extraction of the phenolics. The extraction of phenolics was performed using an ultrasound-assisted extraction method and using ethanol as solvent. The quantitative relation is 1g of ground pineapple peels mixed in 35 mL of ethanol: water solution (50:50% v/v). The UAE method was performed at 25°C for 6.49 mins (Wahab and Yahya, 2019).

After the extraction process, the mixture was filtered using vacuum filtration, and the extract was concentrated using the rotary evaporator at 40°C and a pressure of 175 mbar. The extract was then tested for the presence of phenolics using ferric chloride TS (Shaikh and Patil 2020) and potassium dichromate TS (Ch, et al., 2017).

Synthesis of the Nanoparticles

A stock solution of 50 mL of 0.05 M HAuCl₄ and 50 mL of 0.05 M Zn(CH₃COO)₂ was prepared. Previously prepared 0.5% w/v *A. comosus* peel extract was added dropwise into the mixture of the precursors placed into the ultrasonic bath. The parameters used in the optimization of the synthesis of the bimetallic nanoparticles are the temperature of the ultrasonic bath (60°C, 70°C, 80°C), and the sonication power (60W, 120W, 180W). Table 1 shows the parameters used for each run.

Table 1: Full Factorial Experimental Design of the Synthesis of Au-ZnO BNPs at Different Temperatures and Sonication Power

Run -	Coded Value		Actual Value		
	\mathbf{x}_1	\mathbf{x}_2	\mathbf{x}_1	\mathbf{x}_2	
C1	-1	-1	60°C	60 W	
C2	0	-1	70°C	60 W	
C3	+1	-1	80°C	60 W	
C4	-1	0	60°C	120 W	
C5	0	0	70°C	120 W	
C6	+1	0	80°C	120 W	
C7	-1	+1	60°C	180 W	
C8	0	+1	70°C	180 W	
C9	+1	+1	80°C	180 W	

x₁ = temperature

 x_2 = sonication power

Monometallic nanoparticles of Au and ZnO, which were used as control groups, were also synthesized using the same procedure at 70°C and 180 W sonication power. A change in color of the mixture indicated the formation of nanoparticles.

After the synthesis, the mixture was centrifuged to separate the pellets from the supernatant liquid. The pellets were then washed using deionized water to remove the excess extract adhering to them. The pellets containing the bimetallic nanoparticles were dried in the oven at 50°C and then stored in a vial until use for characterization and assay.

Characterization of the BNPs

The produced bimetallic nanoparticles were characterized by their particle size, morphology, and elemental composition through UV-Vis spectrophotometry, SEM/EDS (Scanning Electron Microscopy/Energy Dispersive X-ray Spectroscopy), and Fourier Transform Infrared Radiation (FTIR).

DPPH Free Radical Scavenging Activity

The DPPH free radical scavenging activity of the nanoparticles was determined by treating 10 μL of varying concentrations (6.25 $\mu g/mL$ to 4000 $\mu g/mL$) of the samples with 190 μL of DPPH reagent in a 96-well plate following a previously published protocol after slight modification (Lee et al. 2015). Ascorbic acid and methanol were considered as the standard and negative controls, respectively. The reaction mixtures were incubated for 30 minutes at 37 °C, and the absorbance was measured at 517 nm using FLUOstar® Omega microplate reader. The scavenging activity in percent (% RSA) was calculated using the equation:

$$\%RSA = \left(1 - \frac{Abs}{Abc}\right) \times 100$$

Where:

Abs denotes the absorbance of the DPPH solution with the sample

Abc denotes the absorbance of the negative control

UV Protection Property

The UV protection property was performed using a UV-Vis spectrophotometer. The assay used 5 $\mu g/mL$ of each sample with DMSO and titanium dioxide as the negative control and reference standard, respectively. The transmission scans were generated from 250 to 800 nm with a 5 nm resolution. The ultraviolet protection factor (UPF) values were calculated according to the transmittance scans from 290 to 400 nm using the equation:

$$UPF = \frac{\int_{290}^{400} E\lambda \times S\lambda \times d\lambda}{\int_{290}^{400} E\lambda \times S\lambda \times d\lambda \times T\lambda}$$

Where:

El denotes relative erythemal spectral effectiveness

SI denotes solar spectral irradiance

dl denotes wavelength step in nm

TI denotes spectral transmittance

Data Analysis

The data were summarized and presented using mean and standard deviation. GraphPad Prism ver. 10.1.1 was used to compute the IC₅₀ for the DPPH scavenging activity of the different Au-ZnO BNPs and the standard. To determine the optimum temperature and sonication power in the experimental range, ANOVA in DesignExpert ver. 22.0.3 was used.

RESULTS AND DISCUSSION

Test for the presence of phenols

Upon the addition of a few drops of 5% ferric chloride solution to the aqueous extract, a dark green or bluish-black coloration was observed, thereby confirming the presence of phenol as per standard qualitative analytical protocols state that the test for phenols is according to how they react with a neutral 1% iron (III) chloride solution. This procedure involves dissolving the chemical in water, or if sparingly soluble, in a hot saturated solution, and then adding a few drops of iron (III) chloride. A phenolic or enolic hydroxyl group is most likely present when there is a temporary or permanent color shift, usually purple, blue, or green (as opposed to yellow or orange). Furthermore, introducing potassium dichromate solution to a separate amount of the extract resulted in the formation of a precipitate. This aligns with the conventional phenol test, which uses 1 mL of a 10% aqueous potassium dichromate solution to treat 5 mL of each solution. Phenolic chemicals are present when a yellowishbrown precipitate forms in the standard test. All of these results point to the extract's phenolic components being present.

Characterization of the BNPs

UV Absorption

To confirm the formation of Au-ZnO BNPs, the synthesized samples underwent characterization using a UV-Visible spectrometer within the wavelength range of 250-800 nm. Fig 2. illustrates the optical absorption spectrum of all synthesized samples, including Au-ZnO BNPs, Au NPs, and ZnO NPs. The monometallic ZnO NPs and Au NPs exhibited absorbance peaks at 315 nm and 545 nm, respectively. In contrast, the Au-ZnO BNPs derived from various temperatures and sonication power levels displayed two distinct characteristic peaks: one between 320 and 345 nm, attributed to the band absorption of ZnO NPs, and another in the visible region between 530 and 540 nm, attributed to the absorption of Au NPs.

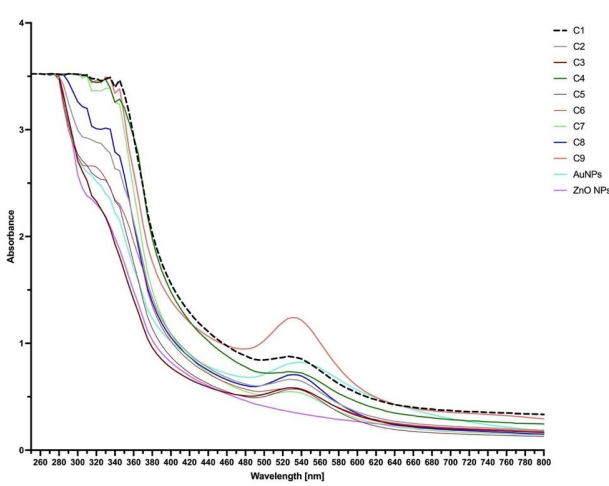


Figure 2: UV absorption of different cases of Au-Zno BNPs, ZnO and Au NPS

SEM Analysis

The morphology, size, and elemental composition of Au-Zno BNPs, Au NPS and ZnO NPs were analyzed using the Scanning Electron Microscope with Energy Dispersive X-ray Spectroscopy (SEM/EDS). The sample consists of different cases of Au-ZnO bimetallic nanoparticles, Au monometallic nanoparticles, and ZnO monometallic nanoparticles formed under various parameters, each distinguished by particular features such as size, shape, and elemental composition, Table 2 elucidated that Case 1 contains spherical nanoparticles of 55 nm in size and made up mostly of carbon (55.59%), oxygen (16.35%), and gold (5.44%). Case 2 has a cuboidal shape at 59 nm, with comparable elemental content but modest percentage differences. Case 3 shows irregular cuboidal nanoparticles at 60 nm with varied elemental ratios. In Cases 4 to 9, the morphology diversifies further, with instances of irregular forms and clusters, and altered chemical composition, including the detection of zinc in other cases.

Table 2: Summary of the Particle Size, Morphology, and Elemental Composition of the Different Nanoparticles

the Different Nanoparticles					
Sample	Parameters	Size	Morphology	Elemental Composition	
Case 1	60°C: 60W	55 nm	Spherical	Carbon 55.59% Oxygen 16.35% Gold 5.44%	
Case 2	70°C: 60W	59 nm	Cuboidal	Carbon 60.97% Oxygen 15.81% Gold 5.13%	
Case 3	80°C : 60W	60 nm	Irregular cuboidal	Carbon 50.27% Oxygen 18.08 % Gold 4.72%	
Case 4	60°C: 120 W	80 nm	Irregular shape	Carbon 62.07% Oxygen 23.35% Gold 4.19%	
Case 5	70°C: 120 W	93 nm	Cluster	Carbon 65.24% Oxygen 19.82% Gold 5.72%	
Case 6	80°C : 120 W	96 nm	Cluster	Carbon 63.24% Oxygen 24.18% Gold 3.29% Zinc 1.27%	
Case 7	60°C: 180 W	99 nm	Spherical	Carbon 64.68% Oxygen 25.38% Gold 2.76% Zinc 0.48%	
Case 8	70°C : 180 W	103 nm	Irregular cuboidal	Carbon 60.13 % Oxygen 24.64% Gold 3.07%	
Case 9	80°C : 180 W	109 nm	Cuboidal	Carbon 62.33 % Oxygen 23.93% Gold 1.93% Zinc 0.29%	
Au NPS	-	75 nm	Cluster	Carbon 55.52% Oxygen 15.49% Gold 5.11%	
ZnO NPs	-	132 nm	Cuboidal	Carbon 52.28% Oxygen 32.17%	

Zinc 0.52%

Fourier Transform Infrared Radiation (FTIR)

The FTIR spectra of various samples of Au-ZnO bimetallic nanoparticles, Au monometallic nanoparticles, and ZnO monometallic nanoparticles present significant data on their chemical compositions and properties. As seen in Figure 2, significant peaks at 3276.43 – 3311.44 cm⁻¹ and 1636.64 – 1637.08 cm⁻¹ may be attributed to the stretching and bending, respectively, of the O-H bonds in the deionized water.

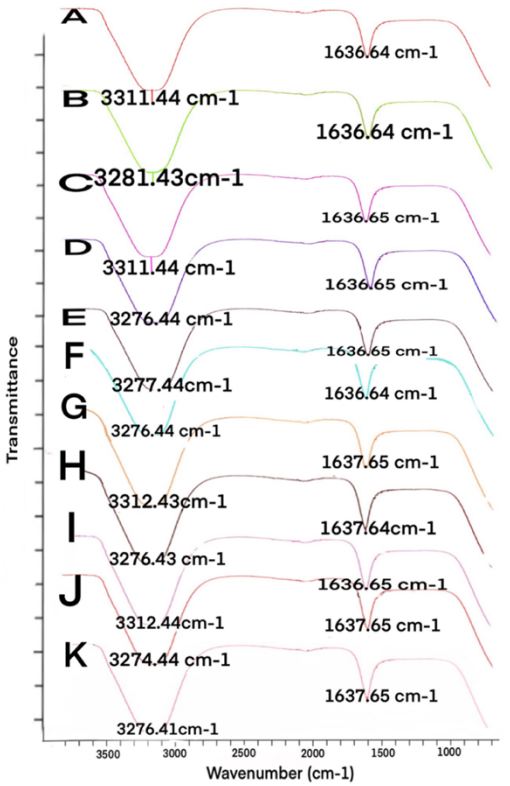


Figure 3: FTIR results of Au-ZnO BNPS, Au NPS and ZnO NPS

In-vitro Assays

DPPH Free Radical Scavenging Activity

The antioxidant properties of the different bimetallic nanoparticles (BNPs) and the standard were assessed using the DPPH assay. The antioxidant activity was indicated by a color change in the solution from deep violet to pale yellow. This change occurs due to the reaction of DPPH radicals with a sample capable of donating hydrogen atoms, resulting in the reduced form, hydrazine (DPPH-H), which decreases the color intensity (Gulcin and Alwasel 2023). Table 3 displays the IC50 values and ascorbic acid equivalents for each sample. Among the samples, C1 and ZnO NPs exhibited the lowest IC50 values of 11.26 μg/mL and 67.68 μg/mL, respectively, showing greater potency compared to ascorbic acid, which has an IC50 of 74.53 μg/mL. This suggests that C1 and ZnO NPs are more effective in donating hydrogen atoms than other samples. In contrast, C6 had the highest IC50 of 808.68 µg/mL, indicating the lowest antioxidant potency and activity.

Table 3: The IC50 of nine cases Au-Zno Bimetallic Nanoparticles and their Ascorbic Acid equivalent

Sample	IC50	AA Equivalent (mg AA per g Extract)
C1	11.26	739.39
C2	634.39	144.59
C3	250.40	348.69
C4	315.90	344.38
C5	577.86	190.99

C6	808.68	96.53
C7	535.37	156.53
C8	412.15	258.49
C9	393.94	227.85
AuNPS	346.38	218.46
ZnO NPS	67.68	1339.00
Ascorbic Acid	74.53	

UV Protection Property

UV-Vis spectrophotometer analysis was conducted to evaluate the UV protection properties of the Au-ZnO nanoparticles and the standard, TiO₂ (See Fig. 4 and Fig. 5). This measures the ability of the nanoparticles to absorb and scatter UV radiation. Among the samples, C1, C4, C7, and C9 exhibited good UV protection property (See Table 4). These UV blocking capabilities may be attributed to the size and shape of the nanoparticles. The smaller particle size and irregular shape of the nanoparticles correlateto an increase in surface area, leading to stronger UV absorption and scattering properties, which makes them effective in blocking harmful UV rays (Li et al. 2010; Shard et al. 2018).

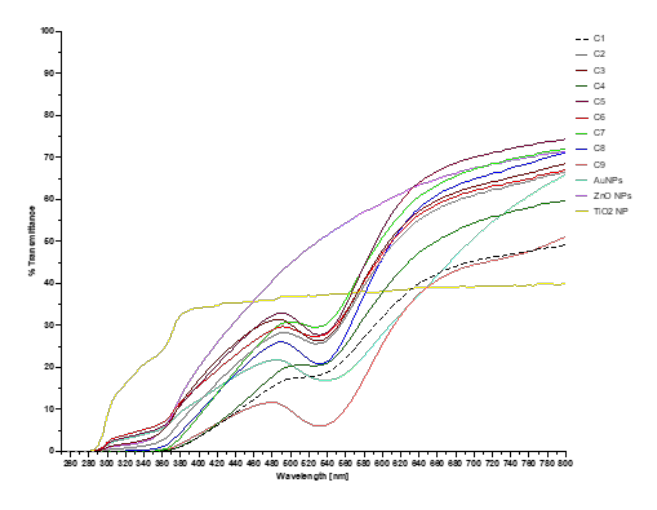


Figure 4: UV transmittance spectra of the different Au-ZnO BNPS and the controls at 250 – 800 nm

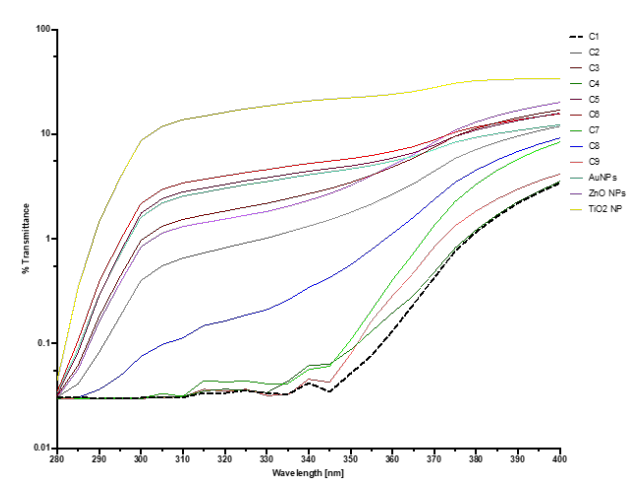


Figure 5: UV transmittance spectra of the different Au-ZnO BNPS and the controls at $280-400\ \text{nm}$

Table 4: Mean UV Protection Factor (UPF) of the Different NPS

				UV
Sample	UPF_{UVA}	UPF_{UVB}	UPF	Protection
_				Category
C1	15.09	32.45	18.96	Good
	(3.92)	(1.19)	(3.15)	protection
C2	8.82	22.59	11.83	Insufficient
	(7.87)	(18.14)	(9.93)	protection
C3	1.39	13.38	4.33	Insufficient
	(1.17)	(11.46)	(3.69)	protection
C4	13.97	32.20	18.08	Good
	(5.23)	(0.87)	(4.10)	protection
C5	5.49	20.51	8.96	Insufficient
	(5.17)	(17.48)	(7.89)	protection
C6	8.57	21.64	11.41	Insufficient
	(8.97)	(18.50)	(10.55)	protection
C7	9.93	30.87	14.79	Good
	(0.80)	(0.60)	(0.86)	protection
C8	6.37	23.05	10.35	Insufficient
	(4.78)	(12.84)	(6.63)	protection
C9	12.57	32.16	17.02	Good
	(0.82)	(0.63)	(0.69)	protection
Au	4.52	18.55	7.70	Insufficient
NPS	(5.22)	(16.34)	(7.40)	protection
ZnO	1.44	9.68	3.42	Insufficient
NPS	(1.48)	(8.69)	(3.17)	protection
TiO2	0.05	0.24	0.10	Insufficient
NPS	(0.02)	(0.11)	(0.04)	protection

^{*}Presented as mean (SD)

Optimization of the Sonication Temperature and Power

The optimization of the sonication temperature and power during the green-synthesis of the BNPs was determined according to the analyzed critical quality attributes (CQAs) using ANOVA in DesignExpert. Table 5 shows the analysis of the ANOVA model for the prediction of DPPH scavenging activity (IC $_{50}$) and UV protection property (UPF). The Model F-value indicates whether the model terms are significant. In this case, the sonication temperature and power are significant model terms for IC $_{50}$ (F=4.28; p=0.0077) and UPF (F=5.43; p=0.0497).

Table 5: Summary of ANOVA model for the Different Response Factors

Response factor	ANOVA		Fit statistics		
	F- value	Prob>F	\mathbb{R}^2	Adeq. Prec	C.V %
IC50	4.28	0.0077	0.5049	6.8534	83.91
UPF	5.43	0.0497	0.7650	7.5647	22.80

Adequate Precision measures the signal-to-noise ratio. A ratio greater than 4 is desirable. A ratio of 6.8534 and 7.5647 for IC_{50} and UPF, respectively, indicates an adequate signal. Hence, the obtained models can be used to navigate the design space.

Final equation for IC₅₀

 $\begin{array}{lll} IC50 = -16310.97 + 390.93*Temperature + 43.75*Sonication \\ Power & - & 0.32*Temperature*Sonication & Power & - \\ 2.40*Temperature^2 - 0.08*Sonication & Power^2 \\ \end{array}$

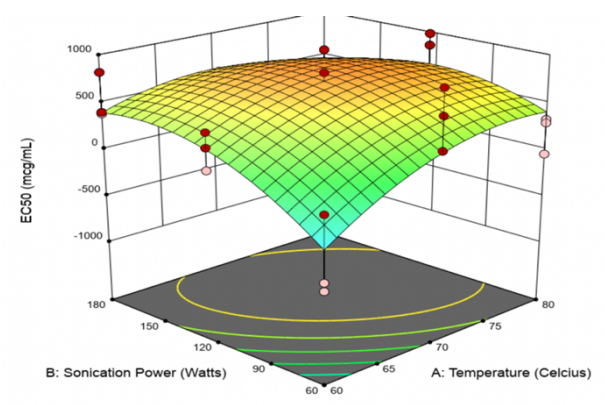


Figure 6: Front View Response surface plot showing the effect of sonication power and temperature on IC50

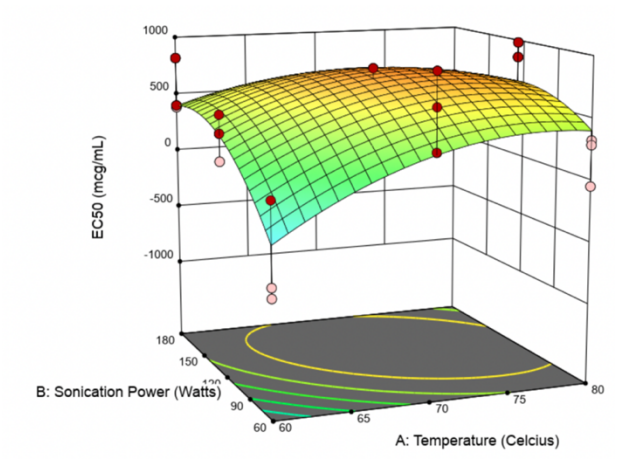


Figure 7: Back View of Response surface plot showing the effect of sonication power and temperature on IC50

Final equation for UPF

UPF = 91.77 - 1.16*Temperature - 0.47*Sonication Power + 0.007*Temperature*Sonication Power

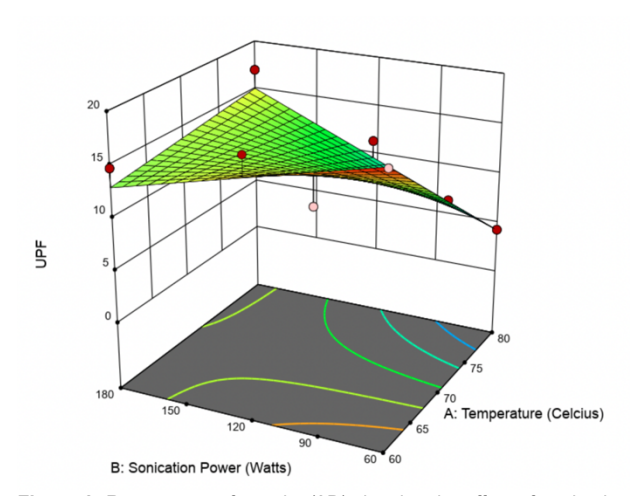


Figure 8: Response surface plot (3D) showing the effect of sonication power and temperature on the UV protection property of the Au-ZnO BNPS

As shown in Fig. 6 to 8, the DPPH scavenging activity and UV protection property increased with the decrease in temperature (60°C) and decrease in sonication power (60 watts). An increase in sonication power leads to more energy dissipation to the system, thereby producing a significantly higher cavity collapse pressure generating smaller droplets (Ruiz et al. 2022). Although studies showed that increase in ultrasonic power decreases particle size, the application of a large enough ultrasonic power promotes growth of the nanoparticles rather than enhance particle refinement (Yang et al. 2021). This may be due to the

increase in temperature caused by the high energy or sonication power. This increase in temperature expands the medium leading to the production of less energetic shock waves (Ruiz et al. 2022). The Au-ZnO BNPs synthesized under 60°C and 60 watts obtained the maximum desirability of 1.0 and was selected as the optimized BNPs.

DISCUSSION

Phenols in the pineapple peel extract were analyzed qualitatively using two standard tests: reaction with neutral 1% iron (III) chloride solution, which produces purple, blue, or green coloration when phenolic or enolic groups are present, and reaction with 10% potassium dichromate solution, which produces a yellowish-brown precipitate confirming phenolic compounds. The presence of phenols in pineapple peel extracts was confirmed by a dark-green or bluish black coloration in the ferric chloride test and precipitate formation in the potassium dichromate test. The Au-ZnO BNPs were dark violet and spherical. The nanoparticles demonstrated an aggregate-like spherical morphology under SEM. Moreover, some of the Au-ZnO BNPs possess gold, zinc, and oxygen upon elemental analysis by SEM-EDX. The UV-Vis spectroscopy analysis revealed distinct absorption features for the synthesized nanoparticles. ZnO NPs exhibited an absorption peak at 315 nm, while Au NPs showed a peak at 545 nm. In contrast, Au-ZnO BNPs displayed two characteristic peaks, one associated with ZnO NPs absorption between 320 and 345 nm, and another in the visible spectrum between 530 and 540 nm attributed to Au NPs absorption. These observations conclusively confirm the successful synthesis of Au-ZnO BNPs, affirming the coexistence and optical characteristics of both Au and ZnO constituents within the NPs.

The synthesized Au-ZnO bimetallic nanoparticles (BNPs) exhibited sizes ranging from 55 to 132 nm. This size range is significant because nanoparticle toxicity is often size-dependent. For instance, smaller nanoparticles tend to penetrate biological membranes more readily, potentially leading to increased cytotoxicity. However, particles within the 50–100 nm range have been shown to have reduced toxicity compared to their smaller counterparts. Specifically, studies have indicated that 50 nm ZnO nanoparticles exhibit lower cytotoxicity than larger particles, such as those at 100 nm or in micrometric sizes (Mitjans et al., 2023). Similarly, gold nanoparticles (AuNPs) larger than 20 nm have demonstrated minimal genotoxic effects, whereas smaller AuNPs (e.g., 5 nm) have been associated with increased DNA damage (Xia et al. 2016).

Furthermore, the green synthesis method employed in this research used pineapple peel extract as a reducing and stabilizing agent, eliminating the need for toxic chemicals commonly used in traditional synthesis methods. This approach not only reduces environmental impact but also enhances the biocompatibility of the nanoparticles. Green-synthesized nanoparticles have been reported to be more stable and less toxic than those produced via conventional methods (Diskhit et al., 2021). By avoiding hazardous reagents and high-energy processes, the green synthesis method contributes to the development of safer nanoparticles with potential pharmaceutical applications.

The antioxidant activity of Au-ZnO BNPs was evaluated using the DPPH assay, in which Case 1, synthesized at a temperature of 60 degrees Celsius and power of 60 watts, achieved the highest antioxidant activity among all the synthesized BNPs. Moreover, the synthesized BNPs with the lowest antioxidant activity were exhibited by Case 6, synthesized at 80 degrees Celsius and 120 watts.

The evaluation of UV protection properties found that Au-ZnO BNPs in Case 1, Case 4, and Case 7 provided superior UV protection compared to TiO2, with the highest UPF values. These cases were synthesized at a constant 60°C sonication temperature with varying power levels. UV-visible transmittance spectra confirmed their effective protection, especially strong against harmful UV-B rays.

Overall, the different cases of Au-ZnO BNPs were investigated to observe which of the temperature and sonication power had the capacity to synthesize Au-ZnO BNPs with the highest antioxidant and UV protection activity using IC50 and UPF values, respectively. The optimal temperature is 60 degrees Celsius, and the optimal sonication power is 60 watts.

The tests carried out in this study confirm the presence of phenolic components in the extract. Adding ferric chloride resulted in dark green or bluish-black coloration, indicating the presence of phenols. These chemicals form colorful complexes with ferric ions (Fe³⁺) due to hydroxyl group reactivity. The addition of potassium dichromate yielded additional confirmation in the form of a precipitate. Potassium dichromate, a strong oxidizing agent, interacts with phenols to create insoluble oxidation products that precipitate out of solution, confirming the presence of the phenolic compounds in the extract

These findings are consistent with previous studies on pineapple fruit, which is known to contain bioactive substances such as organic acids, phenolic compounds, and flavonoids. For instance, (Lasunon et al. 2022) discovered that pineapple peel extract contains a higher concentration of phenolic compounds compared to the core and pomace extracts. Similarly, (Tlais et al. 2020) found that beneficial compounds such as polyphenols are often more abundant in the waste parts of fruits and vegetables than in the edible areas. Notably, these phenolic compounds not only contribute to antioxidant and biological activities but also assist in the formation of metallic nanoparticles.

Building on this understanding of phenolic compounds, UV-Visible spectroscopy was used to assess the formation of Au-ZnO bimetallic nanoparticles (BNPs). The spectral analysis showed distinct absorbance peaks for both the ZnO and gold components, confirming the presence of each element in the bimetallic system. ZnO nanoparticles exhibited a typical absorbance peak at 315 nm due to band-gap absorption, while gold nanoparticles showed a peak at 545 nm corresponding to surface plasmon resonance (SPR).

Furthermore, the Au-ZnO BNPs revealed two distinct peaks: one between 320 and 345 nm for ZnO and another between 530 and 540 nm for gold. This shift in the ZnO band position is attributed to gold's electronegativity, which alters the electron density in ZnO, thereby changing its electronic characteristics. The observed reduction in ZnO's absorbance strength in some bNP samples suggests that gold is present on the surface of the ZnO nanoparticles, which aligns with previous findings by Fageria et al. (2014), demonstrating successful gold integration onto ZnO nanoparticles (Fageria et al. 2014).

In addition to confirming nanoparticle synthesis, the elemental analysis of the Au-ZnO BNPs provided further evidence of the presence of gold, zinc, and oxygen in the samples. However, zinc was occasionally found in lower quantities, likely due to the lower volume percentage of Zn in comparison to Au. This observation was also consistent with the UV-Vis analysis, which showed a decrease in the ZnO absorbance peaks.

Temperature and ultrasonic power are key parameters influencing nanoparticle nucleation and growth. As noted by

Sasani et al. (2017), higher temperatures decrease the supersaturation of the precursor solution, leading to larger nuclei and faster nanoparticle growth. In line with this, increasing temperatures for the Au-ZnO nanoparticle synthesis process resulted in larger nanoparticles due to enhanced mobility and availability of precursor materials (Sasani et al. 2017).

Similarly, ultrasonic power plays a critical role in determining particle size. (Yang et al. 2021) demonstrated that particle size is inversely proportional to ultrasonic power. Although increased ultrasonic power generally leads to smaller particles, once a certain threshold is reached, the rate of size reduction slows, and excessive power can actually promote particle growth rather than refinement.

Following the optimization of synthesis parameters, the antioxidant properties of the Au-ZnO BNPs were assessed using the DPPH scavenging assay. The results revealed that nanoparticles synthesized at 60°C and 60 watts demonstrated the highest antioxidant activity, with lower IC50 values indicating increased radical scavenging potential. Notably, sample C1, which had the smallest particle size, exhibited the strongest antioxidant activity due to its greater surface area, allowing more active sites for interaction with free radicals. Conversely, sample C6 had the lowest activity, likely due to fewer available active sites for radical interaction.

These results highlight the significance of nanoparticle size in determining antioxidant efficiency, as both temperature and ultrasonic power influence the resulting particle size and, consequently, the biological activity of the nanoparticles.

In addition to their antioxidant potential, the UV extinction analysis further confirmed the UV protective properties of the nanoparticles. Nanoparticles with high extinction coefficients in the UV region demonstrated strong absorption and scattering capabilities, which are crucial for blocking harmful UV radiation and providing enhanced protection against UV-induced damage.

To assess the UV protective efficacy of the Au-ZnO nanoparticles, UV-Vis spectrophotometer analysis was performed alongside a standard reference, TiO₂. Samples C1, C4, C7, and C9 had better UV protection and provided support to the concept that larger surface areas and surface-to-volume ratios enhance nanoparticle reactivity. UV radiation is more efficiently absorbed and dispersed by nanoparticles having a greater surface area.

This explains why spherical nanoparticles (Case 1, 55 nm) were effective at protecting against UV light because of their high surface-to-volume ratio, stability, uniformity, and reactivity. Similar to this, the cuboidal nanoparticles (Case 2, 59 nm) had a little lower surface-area-to-volume ratio and were marginally less reactive. They also demonstrated intermediate stability and homogeneity, making them appropriate in certain applications for particular interactions. However, despite their decreased stability and aggregation potential, irregular nanoparticles (Cases 3 to 9) also offered improved UV protection because of their higher surface area, which raised their reactivity.

This confirmed that reactivity improves with decreasing particle size and increasing surface-to-volume ratio, resulting in excellent UV-blocking effectiveness. The fine balance between size, stability, and reactivity in the design of nanomaterials is demonstrated by the fact that irregular nanoparticles provide excellent UV protection while spherical nanoparticles give stable and predictable reactivity.

This relationship between nanoparticle morphology and UV protection emphasizes the importance of optimizing size and

shape when designing materials for enhanced UV shielding. For example, gold nanoparticles (Au NPs) are known for their UV-blocking capabilities, while zinc oxide nanoparticles (ZnO NPs) are recognized for their ability to block both UVA and UVB rays. When combined, these materials formed bimetallic nanoparticles (Au-ZnO BNPs), which provide better UV protection by significantly absorbing harmful UV rays and reducing the transmittance of both UVA and UVB radiation.

Finally, as shown in Fig. 5 to 7, the DPPH scavenging activity and UV protection property increased with the decrease in temperature (60°C) and decrease in sonication power (60 watts). An increase in sonication power leads to more energy dissipation to the system, thereby producing a significantly higher cavity collapse pressure, generating smaller droplets (Ruiz, et al., 2022). Although studies showed that an increase in ultrasonic power decreases particle size, the application of a large enough ultrasonic power promotes the growth of the nanoparticles rather than enhancing particle refinement (Yang et al. 2021). This may be due to the increase in temperature caused by the high energy or sonication power. This increase in temperature expands the medium leading to the production of less energetic shock waves (Ruiz et al. 2022). The Au-ZnO BNPs synthesized under 60°C and 60 watts obtained the maximum desirability of 1.0 and was selected as the optimized BNPs.

CONCLUSION

In the present study, an environmentally friendly and rapid ultrasonic-assisted green synthesis approach was used to synthesize Au-ZnO bimetallic nanoparticles (BNPs) using pineapple peel extract. The particle size, yield, and antioxidant and UV protective properties were influenced by different conditions, including ultrasonic temperature and power.

The findings revealed that ultrasonic temperature is a significant predictor of both antioxidant and UV protective properties of Au-ZnO BNPs. Additionally, ultrasonic power significantly impacts the antioxidant properties. Under the optimal reaction conditions of 60°C and an ultrasonic power of 60 W, the synthesized Au-ZnO BNPs exhibited the highest antioxidant and UV protective properties. Furthermore, Au-ZnO BNPs synthesized under these optimal conditions demonstrated superior antioxidant and UV protective properties compared to individually synthesized Au and ZnO MNPs. Therefore, the study demonstrates the correlation between ultrasonic conditions and the enhanced antioxidant and UV protective properties of Au-ZnO BNPs, as evidenced by the conducted in vitro assays.

ACKNOWLEDGMENT

This study was supported by the Center for Research and Development of Adamson University.

CONFLICT OF INTEREST

The authors declare that there is no conflict of interest.

CONTRIBUTIONS OF INDIVIDUAL AUTHORS

Conception and design of study: A.M. Lapuz, J.D. Fundano Acquisition of funding: A.M. Lapuz, J.D. Fundano Acquisition of data: J.M. Bañes, J.D.G. Contreras, F. E. Nour, Q.T. Trinidad, A.M. Lapuz, J.D. Fundano

Analysis and/or interpretation of data: Q.T. Trinidad, J.D.G. Contreras, A.M. Lapuz, J.D. Fundano Draft of the manuscript: J.M. Bañes, J.D.G. Contreras, F. E. Nour, Q.T. Trinidad, A.M. Lapuz, J.D. Fundano Revision of the manuscript: J.M. Bañes, J.D.G. Contreras, F. E. Nour, Q.T. Trinidad, A.M. Lapuz, J.D. Fundano

REFERENCES

- Abdussalam-Mohammed, W. (2019). Review of Therapeutic Applications of Nanotechnology in Medicine Field and its Side Effects. Journal of Chemical Reviews, 1(3), 243–251. https://doi.org/10.33945/sami/jcr.2019.3.5
- Afreen, A., Ahmed, R., Mehboob, S., Tariq, M., Alghamdi, H. A., Zahid, A. A., Imran, A., & Malik, K. (2020). Phytochemical-assisted biosynthesis of silver nanoparticles from Ajuga bracteosa for biomedical applications. *Materials Research Express*, 7(7), 075404. https://doi.org/10.1088/2053-1591/aba5d0
- Ak, K., Rashid, R., Murtaza, G., & Zahra, A. (2014). Gold nanoparticles: Synthesis and applications in drug delivery. *Tropical Journal of Pharmaceutical Research*, *13*(7), 1169. https://doi.org/10.4314/tjpr.v13i7.23
- Al-Jbour, N. (2022). Enhanced oral bioavailability through nanotechnology in Saudi Arabia: A meta-analysis. *Arabian Journal of Chemistry*, 15(4), 103715. https://doi.org/10.1016/j.arabjc.2022.103715
- Bayda, S., Adeel, M., Tuccinardi, T., Cordani, M., & Rizzolio, F. (2019). The History of Nanoscience and Nanotechnology: From Chemical–Physical Applications to Nanomedicine. Molecules, 25(1), 112. https://doi.org/10.3390/molecules25010112
- Berţa, L., Coman, N., Rusu, A., & Tănase, C. (2021). A review on Plant-Mediated Synthesis of bimetallic nanoparticles, characterisation and their biological applications. Materials, 14(24), 7677. https://doi.org/10.3390/ma14247677
- Bisso, S., & Leroux, J. (2020). Nanopharmaceuticals: A focus on their clinical translatability. International Journal of Pharmaceutics, 578, 119098. https://doi.org/10.1016/j.ijpharm.2020.119098
- Cao, X., Mirjalili, A., Wheeler, J. R., Xie, W., & Jang, B. W. (2015). Investigation of the preparation methodologies of Pd-Cu single atom alloy catalysts for selective hydrogenation of acetylene. Frontiers of Chemical Science and Engineering, 9(4), 442–449. https://doi.org/10.1007/s11705-015-1547-x
- Ch, D., Naga, N., Srinivasa, P., & Afzal, S. (2017). Biological evaluation of *Merremia emarginata* for antibacterial, antifungal, and antioxidant activities. *World journal of Pharmacy and pharmaceutical sciences*, 1509-1525. DOI: 10.20959/wjpps20177-9571
- Cruz, D., Falé, P. L., Mourato, A., Vaz, P. D., Serralheiro, M. L., & Lino, A. (2010). Preparation and physicochemical characterization of Ag nanoparticles biosynthesized by Lippia citriodora (Lemon Verbena). *Colloids and Surfaces B: Biointerfaces*, 81(1), 67–73. https://doi.org/10.1016/j.colsurfb.2010.06.025.
- Dewi, Y., & Simamora, C. (2023). Pineapple (Ananas comosus [L.] Merr.) Cv. Queen-peel herbal tea with a variety of drying temperatures: bioactive compounds, antioxidant activity and

- antimicrobial activity. *Food Research*, 7(4), 344–351. https://doi.org/10.26656/fr.2017.7(4).005
- Ding, L., Yao, C., Yin, X., Li, C., Huang, Y., Wu, M., Wang, B., Guo, X., Wang, Y., & Wu, M. (2018). Size, shape, and protein corona determine cellular uptake and removal mechanisms of gold nanoparticles. *Small*, *14*(42). https://doi.org/10.1002/smll.201801451
- Diskhit, P., Kumar, J., Das, A., Sadhu, S., Sharma, S., Singh, S., Gupta, P., & Kim, B. (2021). Green synthesis of metallic nanoparticles: applications and limitations. *Catalysts*, 11(8), 902. https://doi.org/10.3390/catal11080902
- Ernsting, M. J., Murakami, M., Roy, A., & Li, S. (2013). Factors controlling the pharmacokinetics, biodistribution, and intratumoral penetration of nanoparticles. Journal of Controlled Release, 172(3), 782–794. https://doi.org/10.1016/j.jconrel.2013.09.013
- Fageria, P., Gangopadhyay, S., & Pande, S. (2014). Synthesis of ZnO/Au and ZnO/Ag nanoparticles and their photocatalytic application using UV and visible light. *RSC Advances*, *4*(48), 24962–24972. https://doi.org/10.1039/c4ra03158j
- Freitas de Oliveira, C., Giordani, D., Lutckemier, R., Gurak, P. D., Cladera-Olivera, F., & Ferreira Marczak, L. D. (2016). Extraction of pectin from passion fruit peel assisted by ultrasound. LWT Food Science and Technology, 71, 110–115. doi:10.1016/j.lwt.2016.03.027
- Gao, L., Mei, S., Ma, H., & Chen, X. (2022). Ultrasound-assisted green synthesis of gold nanoparticles using citrus peel extract and their enhanced anti-inflammatory activity. *Ultrasonics Sonochemistry*, 83, 105940. https://doi.org/10.1016/j.ultsonch.2022.105940
- Gulcin, I. and Alwasel, S.H. (2023). DPPH Radical Scavenging Assay. *Processes*, 11(8), 2248. https://doi.org/10.3390/pr11082248
- Iravani, S. (2011). Green synthesis of metal nanoparticles using plants. Green Chemistry, 13(10), 2638–2650. https://doi.org/10.1039/C1GC15386B
- Iravani, S., Korbekandi, H., Mirmohammadi, S. V., & Zolfaghari, B. (2014). Synthesis of silver nanoparticles: chemical, physical and biological methods. Research in pharmaceutical sciences, 9(6), 385–406
- Karadirek, Ş., & Okkay, H. (2019). Ultrasound-assisted green synthesis of silver nanoparticle-attached activated carbon for levofloxacin adsorption. Journal of the Taiwan Institute of Chemical Engineers. doi:10.1016/j.jtice.2019.10.007
- Khairunnisa, S., Wonoputri, V., & Samadhi, T. W. (2021). Effective deagglomeration in biosynthesized nanoparticles: a mini review. *IOP Conference Series*, *1143*(1), 012006. https://doi.org/10.1088/1757-899x/1143/1/012006.up
- Lasunon, P., Phonkerd, N., Tettawong, P., & Sengkhamparn, N. (2022). Total phenolic compound and its antioxidant activity of by-product from pineapple. *Food Research*, *6*(4), 107–112.
- Lee, K. J., Oh, Y. C., Cho, W. K., & Ma, J. Y. (2015). Antioxidant and Anti-Inflammatory Activity Determination of One Hundred Kinds of Pure Chemical Compounds Using Offline and Online Screening HPLC Assay. Evidence-based complementary and alternative medicine: eCAM, 2015, 165457. https://doi.org/10.1155/2015/165457

- Li, Q., Xia, L., Zhang, Z., & Zhang, M. (2010). *Ultraviolet Extinction and Visible Transparency by Ivy Nanoparticles*. *Nanoscale Research Letters*, 5(9), 1487–1491. doi:10.1007/s11671-010-9666-2
- Makarov, V. V., Love, A. J., Sinitsyna, O. V., Makarova, S. S., Yaminsky, I. V., Taliansky, M. E., & Kalinina, N. O. (2014). "Green" nanotechnologies: synthesis of metal nanoparticles using plants. *Acta naturae*, *6*(1), 35–44.
- Micheletti, C., & Venturini, M. (2015). Regulation and safety. Nutrafoods. https://doi.org/10.1007/s13749-015-0038-5
- Milanezi, F. G., Meireles, L. M., Scherer, R., De Oliveira, J. P., Da Silva, A. R., De Araújo, M. L., Endringer, D. C., Fronza, M., & Guimarães, M. C. C. (2019). Antioxidant, antimicrobial and cytotoxic activities of gold nanoparticles capped with quercetin. *Saudi Pharmaceutical Journal*, *27*(7), 968–974. https://doi.org/10.1016/j.jsps.2019.07.005
- Mirzaei, H., & Darroudi, M. (2017). Zinc oxide nanoparticles: Biological synthesis and biomedical applications. Ceramics International, 43(1), 907–914. https://doi.org/10.1016/j.ceramint.2016.10.051
- Mitjans, M., Marics, L., Bilbao, M., Maddaleno, A. S., Piñero, J. J., & Vinardell, M. P. (2023). Size matters? A comprehensive in vitro study of the impact of particle size on the toxicity of ZNO. *Nanomaterials*, *13*(11), 1800. https://doi.org/10.3390/nano13111800
- Nagar, V., Singh, T., Tiwari, Y., Aseri, V., Pandit, P. P., Chopade, R. L., Pandey, K., Lodha, P., & Awasthi, G. (2022).
 ZnO Nanoparticles: Exposure, toxicity mechanism and assessment. *Materials Today Proceedings*, 69, 56–63. https://doi.org/10.1016/j.matpr.2022.09.001
- Nasrollahzadeh, M., Mahmoudi-Gom Yek, S., Motahharifar, N., & Ghafori Gorab, M. (2019). Recent Developments in the Plant-Mediated Green Synthesis of Ag-Based Nanoparticles for Environmental and Catalytic Applications. *Chemical record (New York, N.Y.)*, 19(12), 2436–2479. https://doi.org/10.1002/tcr.201800202
- Niżnik, Ł., Noga, M., Kobylarz, D., Frydrych, A., Krośniak, A., Kapka-Skrzypczak, L., & Jurowski, K. (2024). Gold Nanoparticles (AUNPs)—Toxicity, Safety and Green Synthesis: A Critical Review. *International Journal of Molecular Sciences*, 25(7), 4057. https://doi.org/10.3390/ijms25074057
- Padilla-Cruz, A. L., Garza-Cervantes, J. A., Vasto-Anzaldo, X. G., García-Rivas, G., León-Buitimea, Á., & Morones-Ramírez, J. R. (2021). Synthesis and design of Ag–Fe bimetallic nanoparticles as antimicrobial synergistic combination therapies against clinically relevant pathogens. Scientific Reports, 11(1). https://doi.org/10.1038/s41598-021-84768-8
- Pal, R. K., Panigrahi, S., Bhattacharyya, D., & Chakraborti, A. S. (2013). Characterization of citrate-capped gold nanoparticle-quercetin complex: Experimental and quantum chemical approach. *Journal of Molecular Structure*, 1046, 153–163. https://doi.org/10.1016/j.molstruc.2013.04.043
- Parveen, K., Banse, V., & Ledwani, L. (2016). Green synthesis of nanoparticles: Their advantages and disadvantages. Nucleation and Atmospheric Aerosols. https://doi.org/10.1063/1.4945168

- Pates, M. D., Walag, A. M. P., & Del Rosario, R. M. (2024). Phytochemical Screening and Antioxidant Activity Evaluation of Selected Philippine Fruit Peels and Pulps. Asian Journal of Biological and Life Sciences, 13(1), 197.
- Pechyen, C., Ponsanti, K., Tangnorawich, B., & Ngernyuang, N. (2021). Waste fruit peel Mediated green synthesis of biocompatible gold nanoparticles. *Journal of Materials Research and Technology*, 14, 2982–2991. https://doi.org/10.1016/j.jmrt.2021.08.111
- Rodríguez-Félix, F., Graciano-Verdugo, A., Moreno-Vásquez, M. J., Lagarda-Díaz, I., Barreras-Urbina, C. G., Armenta-Villegas, L., Olguín-Moreno, A., & Tapia-Hernández, J. A. (2022). Trends in sustainable green synthesis of silver nanoparticles using Agri-Food waste extracts and their applications in health. *Journal of Nanomaterials*, 2022, 1–37. https://doi.org/10.1155/2022/8874003
- Romelle, F.D., Rani, P.A. & Mayahnohar, R.S. (2016) Chemical Composition of Some Selected Fruit Peels. *European Journal* of Food Science and Technology, 4, 12-21.
- Ruiz, E., Orozco, V.H., Hoyos, L.M., and Giraldo, L.F. (2022). Study of sonifaction parameters on PLA nanoparticles preparation by simple emulsion-evaporation solvent technique. *European Polymer Journal*. 173. 111307.
- Sani, A., Cao, C., & Cui, D. (2021). Toxicity of gold nanoparticles (AuNPs): A review. *Biochemistry and Biophysics Reports*, 26, 100991. https://doi.org/10.1016/j.bbrep.2021.100991
- Sasani Ghamsari M, Mehranpour H, Askari M. Temperature effect on the nucleation and growth of TiO2 colloidal nanoparticles. Nanochem Res, 2017; 2(1):132-139. DOI: 10.22036/ncr.2017.01.012
- Satpathy, S., Patra, A., Ahirwar, B., & Hussain, M. D. (2020). Process optimization for green synthesis of gold nanoparticles mediated by extract of Hygrophila spinosa T. Anders and their biological applications. *Physica E-low-dimensional Systems* & *Nanostructures*, 121, 113830. https://doi.org/10.1016/j.physe.2019.113830
- Shaikh, J., & Patil M. (2020). Qualitative tests for preliminary phytochemical screening: An overview. *International Journal of Chemical Studies*. https://doi.org/10.22271/chemi.2020.v8.i2i.8834
- Shard, A. G., Wright, L., & Minelli, C. (2018). Robust and accurate measurements of gold nanoparticle concentrations using UV-visible spectrophotometry. Biointerphases, 13(6), 061002. doi:10.1116/1.5054780
- Sulaiman, S. F., Othman, F., & Yusoff, K. (2018). In vitro antioxidant activities of phenols and oleanolic acid from mango peel and their cytotoxic effect on A549 cell line. Molecules, 23(6), 1395. https://doi.org/10.3390/molecules23061395
- Tajally, M. et al. (2008). Effect of ultrasonic treatment on the particle size and morphology of ZnO nanoparticles. Materials Research Bulletin. https://doi.org/10.1016/j.materresbull.2007.04.005
- Tlais, A.Z.A., Fiorino, G.M., Polo, A., Filannino, P., & Cagno, R.D. (2020). High-Value Compounds in Fruit, Vegetable, and Cereal Byproducts: An Overview of Potential Sustainable

- Reuse and Exploitation. Molecules, 25(13), 2987-3010. https://doi.org/10.3390/molecules25132987
- Tohidi, Z. et al. (2022). Ultrasonic-assisted synthesis of nanoparticles: Influence of sonication parameters. Ultrasonics Sonochemistry.
 - https://doi.org/10.1016/j.ultsonch.2022.105940
- Vu, H. T., Scarlett, C. J., & Vuong, Q. V. (2018). Phenolic compounds within banana peel and their potential uses: A review. Journal of Functional Foods, 40, 238–248. https://doi.org/10.1016/j.jff.2017.11.006
- Wahab R., & Yahya, N. (2019). Ultrasound-assisted extraction of polyphenols from pineapple skin. *AIP Conf. Proc. 2155*. https://doi.org/10.1063/1.5125506
- Wang, W., Ma, X., Xu, Y., Cao, Y., Jiang, Z., Ding, T., & Liu, D. (2015). Ultrasound-assisted heating extraction of pectin from grapefruit peel: optimization and comparison with the conventional method. Food Chemistry, 178, 106e114. http://dx.doi.org/10.1016/j.foodchem.2015.01.080
- Wilhelm, S., Tavares, A. J., Dai, Q., Ohta, S., Audet, J., Dvorak, H. F., & Chan, W. C. W. (2016). Analysis of nanoparticle delivery to tumours. *Nature Reviews Materials*, 1(5). https://doi.org/10.1038/natrevmats.2016.14
- Xia, Q., Li, H., Liu, Y., Zhang, S., Feng, Q., & Xiao, K. (2016). The effect of particle size on the genotoxicity of gold nanoparticles. *Journal of Biomedical Materials Research Part A*, 105(3), 710–719. https://doi.org/10.1002/jbm.a.35944
- Xu, J., Song, M., Zhou, F., Zheng, L., Huang, X., & Liu, K. (2023). Applications and challenges of ultra-small particle size nanoparticles in tumor therapy. Journal of Controlled Release, 353, 699–712. https://doi.org/10.1016/j.jconrel.2022.12.028
- Yang, G., Lin, W., Lai, H., Tong, J., Lei, J., Yuan, M., Zhang, Y., and Cui, C. (2021). Understanding the relationship between particle size and ultrasonic treatment during the synthesis of metal nanoparticles. *Ultrasonics Sonochemistry*, 73. http://doi.org/10.1016/j.ultsonch.2021.105497